



UNIVERSITY OF LEEDS

This is a repository copy of *First evidence of widespread active methane seepage in the Southern Ocean, off the sub-Antarctic island of South Georgia*.

White Rose Research Online URL for this paper:
<http://eprints.whiterose.ac.uk/82703/>

Version: Accepted Version

Article:

Römer, M, Torres, M, Kasten, S et al. (13 more authors) (2014) First evidence of widespread active methane seepage in the Southern Ocean, off the sub-Antarctic island of South Georgia. *Earth and Planetary Science Letters*, 403. 166 - 177. ISSN 1385-013X

<https://doi.org/10.1016/j.epsl.2014.06.036>

Reuse

Unless indicated otherwise, fulltext items are protected by copyright with all rights reserved. The copyright exception in section 29 of the Copyright, Designs and Patents Act 1988 allows the making of a single copy solely for the purpose of non-commercial research or private study within the limits of fair dealing. The publisher or other rights-holder may allow further reproduction and re-use of this version - refer to the White Rose Research Online record for this item. Where records identify the publisher as the copyright holder, users can verify any specific terms of use on the publisher's website.

Takedown

If you consider content in White Rose Research Online to be in breach of UK law, please notify us by emailing eprints@whiterose.ac.uk including the URL of the record and the reason for the withdrawal request.



eprints@whiterose.ac.uk
<https://eprints.whiterose.ac.uk/>

First evidence of widespread active methane seepage in the Southern Ocean

Römer, M.^{1,*}, Torres, M.², Kasten, S.³, Kuhn, G.³, Graham, A.G.C.^{4,5}, Mau, S.¹, Little, C.T.S.⁶, Linse, K.⁵,
5 Pape, T.¹, Geprägs, P.¹, Fischer, D.^{1,3}, Wintersteller, P.¹, Marcon, Y.¹, Rethemeyer, J.⁷, Bohrmann, G.¹
and shipboard scientific party ANT-XXIX/4

¹ *MARUM – Center for Marine Environmental Sciences and Department of Geosciences, University of Bremen, Klagenfurter Str., 28359 Bremen, Germany*

10 ² *College of Oceanic and Atmospheric Sciences, Oregon State University, 104 Ocean Admin Building, Corvallis, Oregon 97331-5503*

³ *Alfred Wegener Institute, Helmholtz Centre for Polar and Marine Research, Am Handelshafen 12, 27515 Bremerhaven, Germany*

⁴ *College of Life and Environmental Sciences, University of Exeter, Rennes Drive, Exeter EX4
15 4RJ, UK*

⁵ *Geological Sciences Division, British Antarctic Survey, High Cross, Madingley Road, Cambridge CB3 0ET, UK*

⁶ *School of Earth and Environment, University of Leeds, Leeds LS2 9JT, UK*

⁷ *Institute of Geology and Mineralogy, University of Cologne, 50674 Cologne, Germany*
20

* *Corresponding author: Phone +49(0)421 218 65059 Fax +49(0)421 218 65099 E-mail: mroemer@marum.de*

25 **Abstract**

A new extensive submarine cold-seep area was discovered on the northern shelf of South Georgia during R/V Polarstern cruise ANT-XXIX/4 in spring 2013. Hydroacoustic surveys and video-based sea floor observations documented the presence of 133 individual gas bubble emissions, which were restricted to glacially-formed fjords and troughs. Effective methane transport from these emissions
30 into the hydrosphere was proven by relative enrichments of dissolved methane in near-bottom waters. Stable carbon isotopic signatures of the methane pointed to a predominant microbial origin. Although known from many continental margins in the world's oceans, this is the first report of an active area of methane seepage in the Southern Ocean. Our finding of substantial methane emission related to a trough and fjord system, a topographical setting that exists commonly in glacially-
35 affected areas, opens up the possibility that methane seepage is a more widespread phenomenon in polar and sub-polar regions than previously thought.

Keywords: Cold seeps, gas bubble emissions, methane seepage, South Georgia

1. Introduction

40 Sea-floor hydrocarbon seepage occurs at numerous sites on the world's ocean margins, from the continental shelves to the abyssal depths, in a variety of geological settings^{1,2}. Notwithstanding several decades of global methane seep exploration, examples in the Southern Ocean are almost unknown. First videographic evidence of an Antarctic cold seep was obtained by Domack et al.³ from the seafloor beneath the collapsed Larsen B ice shelf, western Weddell Sea, located in the trough of
45 the Evans and Crane glacier. This site was later revisited by Niemann et al.⁴, who classified the seepage as inactive, based on the presence of dead shells of seep-associated chemosymbiotic clams (*Calypptogena* sp.), a geochemical sea floor analysis, and the lack of hydroacoustically detectable gas

emissions. Apart from at this single extinct cold seep site, naturally occurring chemosynthetic organisms⁵ have also been found in the Southern Ocean at hydrothermal vents in the Bransfield Strait^{6,7} and the South Sandwich back-arc⁸, and at a whale fall from the Kemp Caldera⁹. The paucity of records of chemosynthesis-based communities in the Southern Oceans can be partly explained by a lack of exploration, due to the challenging and remote conditions in this region¹⁰.

The expanding numbers of seep locations discovered worldwide highlights the importance of methane seepage for the global carbon cycle, and its potential contribution to the oceanic and atmospheric methane inventory, where - in the latter case - methane acts as a potent greenhouse gas. In contrast to deep-water seep sites, where most bubbles dissolve during ascent through the water column and the dissolved methane is oxidized by microbes¹¹⁻¹³, a fraction of gas emitted from shallow water environments may transgress the sea-atmosphere boundary, especially in storm seasons^{14,15}. Therefore, shelf and upper slope areas such as off Spitsbergen^{16,17}, in the Black Sea¹⁸, and off East Siberia¹⁹ are of particular interest when considering the role of methane seepage as a possible contributor to concentrations of methane in the atmosphere.

South Georgia belongs to the crustal blocks forming the North Scotia Ridge (Fig. 1a), which were once part of the continental connection between South America and the Antarctic Peninsula^{20,21}. These crustal blocks were moved during the Cenozoic by backarc spreading and subsequent eastward growth of the Scotia Sea^{20,22}. There is evidence for active convergence along the western side of the North Scotia Ridge, but convergence has now ceased along its eastern section, which includes the South Georgia block^{20,23}. However, analyses of an earthquake with its epicenter located south of the South Georgia block (see Fig. 1b) indicates nearly pure thrust faulting, interpreted to represent thrusting of the Scotia Plate beneath South Georgia²⁴. This tectonic framework shows that South Georgia is part of an isolated microcontinental block, divided by the W-E trending Cooper Bay Shear Zone that crosses the Island (Fig. 1b). This is the major tectonic boundary that displaces the late Jurassic to early Cretaceous basement complexes exposed on South Georgia²⁵.

In contrast to the knowledge of the geologic and tectonic evolution of South Georgia, the shelf and upper slope area surrounding the Island have been less well studied. However, a recent comprehensive bathymetric compilation aimed at elucidating the paleo-ice sheet drainage of the Island has greatly improved our knowledge of the continental shelf morphology of South Georgia²⁶. Graham et al.²⁶ described large eroded troughs linked to the recent fjords around South Georgia (Fig. 1b), and they proposed that these cross-shelf troughs were formed during glacial times and represent former pathways of outlet glaciers and ice streams. While probable Mesozoic sedimentary and volcanic rocks extend beneath the inner shelf of South Georgia, Cenozoic sediments form the outer parts of the continental shelf^{26,27}.

South Georgia is located in the path of the Antarctic Circumpolar Current (ACC). The Polar Front is located to the north and the southern ACC front loops anticyclonically around the island from the south before retroflecting to the east²⁸. The shelf waters of South Georgia often show oceanographic properties that are markedly different from the open waters, indicating that local processes are important in dictating shelf water mass characteristics²⁹. Various shelf-specific processes have been observed, or inferred at South Georgia, and significant interannual variability of the oceanographic conditions on the shelf are known^{29,30}. Whitehouse et al.³¹ reported a surface water warming of up to 2.3°C in 81 years around South Georgia, however, this warming was not recognized in waters deeper than 200 m. In general, the special oceanographic conditions around South Georgia result in a rich ecosystem, with large phytoplankton blooms and related strong atmospheric carbon drawdown^{32,33}, as well as high organic matter sedimentation on the shelf. The seasonally occurring blooms are particularly intense on the northern shelf area of South Georgia and within the adjacent Georgia Basin³².

In this study we performed a comprehensive hydroacoustic survey along the northern shelf of South Georgia, detecting numerous gas flares and analyzing their distribution. Subsequent sea floor visual observations of two of these flares revealed a detailed view of the seep sites. These data were correlated with oceanographic parameters and methane analyses in water column samples that

together illustrate methane-related processes taking place in the local hydrosphere. In addition, gas
100 samples taken from sediment cores from the seep sites were analyzed for their stable carbon
isotopic composition, which allowed us infer the source of the methane fueling them.

Results

Hydroacoustic observations

Hydroacoustic surveys revealed the presence of numerous gas emission sites at water depths
105 between 130 and 390 meters below sea level (mbsl) on the northern shelf of South Georgia in spring
2013. The gas emissions appear as 'flares' in the echograms due to the high impedance contrast of
free gas emanating as bubbles through the water column, which produce a high-backscatter signal
(Fig. 2a). The flares are composed of vertically arranged oblique reflections that image the up-rising
individual bubbles or groups of bubbles, and make them discernible from fish schools. In total, at
110 least 133 individual flares were detected during our study (Figs. 3a and b, supplementary table S1).
The flares showed largely straight and vertical orientation (e.g. the 170-m high 'Cumberland Bay
Flare', Fig. 4c), indicating a lack of strong currents that would be expected to deflect the bubbles
during their rise through the water column. Roughly ~75 % of the flares were less than 100 m high,
with an average of ~70 m (supplementary table S1). However, three flares extended from the sea
115 floor to a height of at least 25 mbsl. The uppermost part of the echograms was disturbed by acoustic
noise that hampered differentiation of gas bubbles from plankton and/or fish. In general, the real
flare height was difficult to determine using Parasound recordings, as the small ~4° opening angle
and a coherent narrowing footprint with decreasing depth impeded the detection of the uppermost
part of the flares when the ship did not pass exactly through the center of the bubble train.

120 Many flares detected were discontinuous or had no connection to the sea floor (Figs. 4a and b). This
observation can be attributed to horizontal deflections of a bubble stream that moves in and out of
the conical Parasound beam, or to pulsing gas bubble streams where the emissions are spatially and
temporally variable. The latter explanation seems to be more likely in this case, as the tall flares

appeared vertical and didn't show strong lateral deflections, although variable current regimes
125 cannot be ruled out entirely.

The temporal variability of the flares was examined by imaging a given location more than once. Four
flares became visible at the same location two times within ca. 14 days, whereas seven other flares
appeared only once, although crossed twice (supplementary table S2). The observations of the flare
appearance and the repeated surveys show that most flares probably are temporally variable on
130 scales of minutes to weeks.

The detected flares were not randomly distributed along the South Georgia margin. They occurred
either within the Cumberland Bay fjord system or within the other incised cross-shelf troughs that
cut through the broad shelf surrounding the island (Fig. 3a). Two fjord systems were inspected for
the occurrence of flares during cruise ANT-XXIX/4: Cumberland Bay was investigated intensively (Fig.
135 3b), whereas Possession Bay was entered once and inspected along only two survey lines. While
numerous flares were observed in the Cumberland Bay region, no indication of gas emissions was
found in Possession Bay. In total, more than 75 flares were detected in both branches of Cumberland
Bay and within the cross-shelf to which the fjord system connects (designated as Trough 5 in Fig. 3b).
Flares were distributed close to the fjord-mouth and within the fjord itself, but were not detected in
140 the innermost parts of the bay close to the glaciers that discharge into the fjord at the coast. A few
flares were found within the ~10 km area seaward of the fjord mouth, and one flare was detected as
far as ~30 km from land. In addition to cross-shelf Trough 5, gas emissions were also found in four of
the seven troughs defined by Graham et al.²⁶ on the northern shelf of South Georgia (Fig. 3a). The
northern shelf was passed for hydroacoustic surveys twice in a roughly two week interval and during
145 both investigations flares were observed to be restricted to the troughs. No flares were detected on
the shallower banks between the cross-shelf troughs and, with the exception of Troughs 2 and 7, all
of the troughs surveyed showed gas emissions.

Sedimentary strata were not visible in subbottom Parasound SLF profiles of the shallow shelf banks (Fig. 4b), but the troughs were characterized by reflections indicating sediment accumulations of up to ~40 m in their centers (Figs. 4a). The reflections were sub-parallel to the sea floor and presumably reflect accumulations of sediment transported from the fjords to the shelf, and deposition within the cross-shelf troughs. Numerous zones of acoustic blanking or acoustically-transparent chimneys that pierced the horizontal reflections were observed for all of the sediment infills within the troughs (Figs. 2b, 4a, b and c), suggesting upward gas migration at these sites. The acoustic chimneys were positioned directly underneath the acoustic flares in the water column in several areas, strongly suggesting that the chimneys are the conduits for channeling free gas through the sediments towards the sea floor, where gas bubbles escape into the water column and form the flares imaged in the Parasound PHF echograms (Figs. 2b, 4a, b and c).

Visual sea floor observations at the 'Cumberland Bay Flare'

An OFOS deployment was conducted at a flare site designated as the 'Cumberland Bay Flare' in order to visually confirm the sea floor origin of the gas flares recorded hydroacoustically (Fig. 4c), and the nature of the surrounding sediments. The sea floor was inspected along an approx. 400 m long track (Fig. 5). Visibility during the OFOS deployment was limited to a few meters because of the highly turbid and sediment-rich meltwater in the fjord and inspections were thus performed with an altitude of ~2 m. The flat sea floor was composed of unconsolidated sediments and detached kelp fronds (Figs. 6a and b), many of which were partially buried. The observed epibenthic invertebrate megafauna included cidaroid and echinoid sea urchins, asteroid starfish, holothurians, hexactinellid sponges, and fish (Fig. 6a).

Numerous centimetre-sized holes were visible in the sea floor along the OFOS track, which were probably produced by endobenthic organisms or may represent the orifices of emanating gas bubbles. Rising gas bubbles were observed at two seep sites during the OFOS deployment, which was guided by flare observations in the water column. Our observations document single gas bubbles emanating from the sea floor without forming continuous bubble streams. During an observation

period of about 40 minutes at the southeastern located seep site (Figs. 5 and 6a), we documented
175 more than 50 events (roughly about each minute), where a single bubble or small groups of 2 or 3
bubbles rose from the seabed. We observed individual rising gas bubbles again at a northwestern
seep site, which is located ~50 m distant from the other and corresponded to a different water
column flare (Figs. 5 and 6b).

At both seep sites the sea floor was covered by centimeter to decimeter-sized, subcircular, whitish
180 material (Fig. 6a and b), occurring either as coherent patches or as collections of several smaller
patches (Figs. 5 and 6a). These patches most probably represent microbial mats indicative of fluid
flow from below. However, we did not see taxonomically higher chemosymbiotic organisms typically
associated with cold seeps in other regions, such as bathymodiolin mussels or vesicomid clams. The
sea floor in two locations where whitish material was observed was slightly elevated and formed
185 topographic mounds up to a few decimeters high (Fig. 6a). Fig. 5 illustrates that the whitish material
is restricted to two areas a few meters in extent, both of which are located at the central foci of the
two flares detected hydroacoustically.

Water column characteristics in Cumberland Bay

Three hydrocasts revealed a general water column stratification and specific differences in
190 hydrological conditions in Cumberland Bay (station CTD-1 close to the 'Cumberland Bay Flare'; CTD-2
close to the 'Grytviken Flare'; see Fig. 3b) and a station seaward of the fjord (CTD-3). A pronounced
surface layer (upper ~20 mbsl) was present at stations CTD-1 and CTD-2 in Cumberland Bay,
characterized by relatively low salinities (<33 PSU), temperatures (<2.8 °C) and beam transmissions
(<80 %). These characteristics suggest that this water mass (not observed at the seaward station;
195 Figs. 7, supplementary Fig. S3) represents plumed meltwater and originates from the melting marine
terminating glaciers that feed the bay (Fig. 3b). Physico-chemical properties varied only slightly with
increasing depth throughout the midwater section. The lower limit of this water mass was found at
~165 mbsl for CTD-2 (located relatively deep within the fjord) and at ~190 mbsl for CTD-1 (located
close to the fjord mouth), suggesting that its vertical extent is spatially variable and may reflect

200 topographically-controlled circulation patterns. Similar water characteristics at all three investigated stations indicate water exchange between Cumberland Bay and the shelf area of South Georgia. The lowermost water mass within and outside Cumberland Bay was characterized by relatively low temperatures ($\sim 2.4 - 1.7^{\circ}\text{C}$) and relative depletions in dissolved oxygen concentrations (6.5 – 5.2 mL/l), but with the highest salinities (up to 34.2 PSU). A markedly lower beam transmission (as low as 205 80% at the bottom) recorded for the near-bottom water mass within the bay, if compared to that at the outer shelf station, might be the result of a higher particulate matter load (see also chapter 4.2).

Strong enrichments in dissolved methane of up to 25.4 nmol/l and 55.6 nmol/l, respectively, were measured in the lowermost water mass characterized by low-beam transmission at the two CTD stations taken in close proximity to the ‘Cumberland Bay Flare’ and the ‘Grytviken Flare’ (Figs. 3b and 210 7). At these stations concentrations of dissolved methane decreased significantly with decreasing depth within the lower 100-120 meters of the water column down to ca. 5 nmol/l (Fig. 7), which is still slightly elevated in contrast to the atmospheric equilibrium (3-3.3 nmol/l). At the outer shelf station, where flares were not detected, dissolved methane concentrations of <5 nmol/l were measured though the whole water column.

215 **Stable carbon isotopic composition of methane**

Stable carbon isotopic analysis of methane in the gas samples extracted from the two sediment cores taken in close proximity to flares (GC-1 within cross-shelf Trough 6; GC-2 in the Cumberland Bay; Figs. 3a and b) revealed strong depletions in ^{13}C , with $\delta^{13}\text{C-CH}_4$ values ranging between -80.2 and -88.9% (V-PDB). The greatest depletion came from a methane sample extracted at ~ 6.5 mbsf from the 220 sediment core GC-2 at the ‘Grytviken Flare’.

Discussion

We detected 133 gas flares at the northern shelf of South Georgia (Fig. 3a) during R/V Polarstern cruise ANT-XXIX/4 in 2013. Visual sea-floor inspections with the high-resolution video camera of the OFOS system confirmed active seepage at the ‘Cumberland Bay Flare’ in the form of rising gas

225 bubbles and white sea-bed patches (Figs. 6a and b) interpreted as microbial mats fueled by methane emission. Hydroacoustically-imaged flares originated from sea floor locations that showed acoustically-blanked chimneys in the underlying sediments. In addition, water samples taken in bottom waters within two flares showed elevated concentrations of dissolved methane (Fig. 7), that proved methane transport by gas bubbles from the sea floor into the hydrosphere.

230 This new finding of methane seepage adds to the long and steadily growing list of seep areas in the world's oceans^{1,2,34}. At high latitudes, seeps are known in the Arctic and sub-Arctic, which have recently sparked particular scientific interest because of their links to permafrost settings¹⁹ with potential global warming effects¹⁶. Hydrothermal vents and cold seeps are known to host specialized faunal communities which are based on chemosynthesis^{5,35}. In the Southern Ocean to date only a few
235 chemosynthetic ecosystems are known¹⁰, including the presently inactive cold seep in the western Weddell Sea, hydrothermal vent fields and a natural whale fall^{3,4,6-9}. The epibenthic invertebrate megafauna observed in the Cumberland Bay area comprises species commonly found around South Georgia³⁶⁻³⁸. Except for the inferred microbial mats chemosynthetic organisms usually found at cold seep sites were not found at the seeps investigated in this study. This might be because of the
240 relatively shallow water depth (~250 mbsl), since the typical animals obligate at cold seeps (e.g. species of vesicomyid clams, bathymodiolin mussels and siboglinid tubeworms) are restricted to aphotic habitats. Explanations for their absence on the continental shelves include the abundance of predators in shallower waters, or competitive exclusion by primary consumers limiting the presence of species dependent on chemoautotrophic symbionts³⁹. The exact depth limit is not precisely
245 resolved⁴⁰, but the shallowest seep communities with the typical obligate species found so far are reported from the Eel River basin, offshore California in ~350 mbsl⁴¹ and in the Sea of Okhotsk in ~370 mbsl³⁹. In our study we detected gas bubble seepage using hydroacoustics in the same depth range (ca. 380 mbsl), but did not investigate these sites visually. Thus, it remains a possibility that typical obligate cold seep animals are present on the deeper shelves around South Georgia.

250 As noted above, the flares detected during ANT-XXIX/4 along the northern shelf of South Georgia are not randomly distributed, but are restricted to the fjords and glacial troughs along the shelf (Fig. 3a), the latter accounting for ~15% of the total shelf area surrounding the island of South Georgia. Detailed surveys are required to determine further distribution and total abundance of such methane seep sites, which is probably significantly higher than the 133 flares we detected during the
255 detailed but still spatially-limited surveys of R/V Polarstern cruise ANT-XXIX/4. A similar observation was made in a hydrocarbon seep area on the Baffin Bay shelf region, where oil and gas seeps were found within glacially-formed troughs seaward of fjord systems^{42,43}. In addition, seepage was inferred to occur in fjords in Spitsbergen⁴⁴ and Norway¹, based on the presence of sea floor pockmarks. Fjords generally appear to represent favorable settings for methane seepage as they are commonly
260 characterized by high sedimentation rates (due to high input from inflowing glaciers or meltwater streams). In addition, in some cases shallow water sills hamper water exchange with open seawater areas and ventilation, favouring anoxic conditions and protecting organic material from rapid microbial decomposition under aerobic conditions, which finally leads to large accumulations of refractory organic matter in the sediments¹. During our study we observed various sill structures in
265 the high-resolution bathymetric maps of the South Georgia fjords, probably representing fjord moraines⁴⁵. However, these do not appear to fully restrict flow (Fig. 3b), as temperature, salinity and concentrations of dissolved oxygen are indeed lower in the bottom waters than in overlying water masses, but the values were similar in magnitude for all three stations, both within and outside the fjord. Therefore, there is no apparent isolation of the deep waters in Cumberland Bay (Figs. 7,
270 supplementary Fig. S3). Bottom water oxygen concentrations within and outside the bay were ~5 mL/l (corresponding to ~220 $\mu\text{mol/l}$), indicating well-oxygenated conditions.

For Cumberland Bay, Platt⁴⁶ estimated the sedimentation rate at $2.8 \times 10^3 \text{ g m}^{-2} \text{ yr}^{-1}$ and an organic matter input of $60 \text{ g carbon m}^{-2} \text{ yr}^{-1}$, providing an ideal setting for shallow biogenic methane production. A biogenic methane source is proven by $\delta^{13}\text{C-CH}_4$ values $< -80 \text{ ‰}$ (V-PDB) for all gas
275 samples collected from the two sediment cores we investigated. Methanogens preferentially

consume substrates depleted in ^{13}C , whereas thermogenic light hydrocarbons by non-selective hydrocarbon cracking are not affected by significant isotope fractionation effects⁴⁷. For a microbial hydrocarbon formation and accumulation both high sedimentation rate and the presence of sufficient amount of organic matter in the sediments is required. South Georgia lies in the eastward
280 flowing ACC, creating a morphological high in the largest meander modifying the Southern ACC front^{28,48}. Due to this particular hydrographic configuration, intensive and regular phytoplankton blooms develop in the area north and northwest of the South Georgia shelf³², leading to both a rich food web⁴⁹, and a high carbon production, which is either exported⁵⁰ or ultimately deposited at the sea floor. Although there is no indication for deeply buried reservoirs of thermogenic gas fueling the
285 gas emission sites investigated in this study, thermogenic gas migration through deep-rooted faults cannot be entirely excluded as the fjords and connecting cross-shelf troughs may have established along lines of structural weakness that could have evolved in association to faults zones²⁶. Unfortunately, there are currently no seismic data imaging the deeper structure of the South Georgia block to test such a hypothesis.

290 Due to the nature of our survey, most of the imaged flares were not centered directly under the vessel, thus, precluding a quantitative assessment of their intensities. However, our observations revealed that (1) most flares are only few tens of meters high, (2) flares often appear episodically and are characterized by discharge in pulses, and (3) flares indicative for individual bubbles or bubble groups are occasionally tilted, so that their sea floor origin could not always be traced (Figs. 4a and
295 b). These data suggest that most of the flares are rather weak and represent discontinuous releases of gas bubble emissions. Visual inspection of the 'Cumberland Bay Flare' one of the most intense flares we imaged (Fig. 4c), showed sporadic gas bubble discharge from the projected flare origin, but also indicated that the sporadic release of individual gas bubbles was sufficient to cause a relatively intense signature in the corresponding echogram. Because our data demonstrate that the flares are
300 temporally variable over minutes to weeks it may be possible that the activity and intensity of the gas emissions may also change seasonally or annually.

The quantity of bubbles and the intensity of seepage on the northern shelf of South Georgia seems to be rather weak in comparison to other seep areas, e.g. Hydrate Ridge^{51,52}, the Makran continental margin¹², Santa Barbara channel⁵³, as well as several seepage areas in the Black Sea⁵⁴⁻⁵⁶, where
305 vigorous gas bubble emissions and/or strong flares have been documented. However, the large number of emission sites as revealed from our flare imaging, in combination with the strong enrichments in dissolved methane, suggests injection of significant quantities of methane into the bottom water in fjords and the cross-shelf troughs of South Georgia, even though each individual seep may contribute only a small amount of methane.

310 Our hydroacoustic data additionally indicate that most gas bubbles released into the water column probably did not reach the upper water layer and atmosphere, but instead dissolved entirely during their ascent. With three exceptions, all 133 flares detected disappeared from the SBES echograms well below the sea surface. Although the geometric limitation of the SBES coverage, particularly at shallow depths, has to be considered, the fraction of methane transported as gas bubbles is not
315 limited only by the maximum bubble rising height, but mainly depends on the effectiveness of gas exchange processes taking place when entering the hydrosphere, due to concentration differences. The proportion of methane initially contained in the bubble is rapidly replaced by dissolved nitrogen and oxygen from the ambient water^{11,57,58}. The rapidity of this process strongly depends on the bubble size, the rising velocity, as well as the composition and conditions of the surrounding medium
320 and the presence of upwelling flows⁵⁹. Several studies have demonstrated that methane escapes the bubbles well before final bubble dissolution^{11,56,60,61}. Our suggestion that most of the methane discharged from the South Georgia northern shelf does not reach the upper water column is additionally strengthened by the relatively low concentrations of dissolved methane (about 5 nmol/l) in the intermediate to uppermost water masses at two hydrocast stations, deliberately acquired
325 close to recorded flares in the Cumberland Bay area (Figs. 3b and 8). Most probably, the strong stratification of the water column, as evidenced by the T-S diagram (supplementary Fig. S3), impedes a regular vertical mixing within Cumberland Bay and the released methane therefore remains within

the bottom water, leading to the observed profiles. A fraction of this methane may be oxidized by microbial activity⁶², so the measured concentrations reflect a balance between methane input and sea-floor consumption within Cumberland Bay and water exchange with the outer shelf water. It is hard to directly correlate water column data with flare strength, but our data agrees with our assumption that the methane transported via gas bubbles rapidly dissolves in the water body, so that most of the dissolved methane remains in the bottom water and that bubbles producing the hydroacoustic flares visible at that sites and reaching 50 m higher into the water column may have been depleted in methane.

We argue that the seepage around South Georgia is spatially related to the glacial trough and fjord system, a setting often occurring in sub-Antarctic regions that need further exploration to characterize the nature, distribution and magnitude of hydrocarbon seepage in this region. Research questions about methane seepage around South Georgia following from our study include: 1) unraveling the relationships between seepage, methane sources and rates of sediment accumulation, as well as the type and amount of organic carbon; 2) evaluating the potential contribution of thermogenic gas in some areas; 3) documentation of the biosphere and biogeochemical processes supported by the methane input; 4) establishing whether some of the deeper seeps support chemosynthetic fauna, and, if present, do they serve as 'stepping stones' for larval distribution of chemosynthesis-based organisms in the Southern Ocean; 5) constructing a carbon budget for the region, which includes source and consumption terms as well as the effect of circulation within and outside the fjords, and the circumstances under which this methane may reach the atmosphere.

Methods

350 Hydroacoustic systems

The data used for this study were acquired during R/V Polarstern cruise ANT-XXIX/4 in March and April 2013⁶³. Bathymetric mapping was performed using an ATLAS Hydrosweep Deep-Sea 320-beam echosounder operating at a frequency of ~15 kHz and covering a swath width about four times the

water depth. Raw data were processed with CARIS 7.0 HIPS and SIPS and the MB-System software⁶⁴
355 and the grids produced were visualized with ESRI ArcMap 10.0, which allowed for inclusion of
additional relevant data to be plotted (e.g. track lines, locations of gas emissions). The cleaned
Hydrosweep data were gridded with a cell size of 25 m. We combined our results with additional
data from earlier cruises of the British Antarctic Survey⁶⁵ (available at
http://www.antarctica.ac.uk/bas_research/data/online_resources/sghd/) and the GEBCO dataset
360 (<http://www.gebco.net/>).

We used the ship-mounted parametric single beam echosounder (SBES) ATLAS PARASOUND for
shallow subbottom imaging. The secondary low frequency (SLF) of about 4 kHz was recorded and
processed online with the software ATLAS PARASTORE. The resulting PS3-files were imported to
SENT (H. Keil, University of Bremen) and the data plotted. In addition, the SBES ATLAS PARASOUND
365 was used for flare detection and imaging, using the primary high frequency (PHF) of about 18 kHz
(Fig. 2a). The transducer opening angle is 4°, resulting in a footprint size of about 7% of the water
depth. PARASOUND data as well as metadata are available at the PANGAEA data repository.

Seafloor observations

The Ocean Floor Observation System (OFOS), a towed underwater system equipped with a high-
370 resolution digital camera (ISITEC, CANON EOS 1Ds Mark III), was used to visually inspect the sea floor
in areas where flares were detected. The camera was programmed to take high-resolution (21
megapixels) photographs of the sea floor every 30 seconds at an altitude of about 1.5 – 2 m relative
to the seabed. Underwater-navigation was achieved using the shipboard IXSEA Posidonia ultra short
baseline system, with an accuracy of 5 – 10 m, and these data were used to establish the OFOS tracks
375 and the positions of each photograph taken.

Water column analyses

Water column properties were studied by repeated hydrocasts with a 24-Niskin water bottle rosette
and a CTD (Seabird, SBE 911+). Using the sensors of the CTD-unit, salinity, temperature, and pressure
data were measured and, in addition, a Sea-Tech transmissometer recorded beam transmission and
380 a SBE 43 sensor concentrations of dissolved oxygen. For quantification of methane concentrations in

the water column, 750 ml of sampled seawater were transferred from the Niskin bottles into pre-evacuated 1000 ml glass bottles immediately after recovery, followed by gas extraction according to the modification of the vacuum degassing method described by Rehder et al.⁶⁶. The extracted gas samples were analyzed with a 6890N gas chromatograph (Agilent Technologies) equipped with a capillary column and connected to a Flame Ionization Detector, as described in Pape et al.⁵⁵.
385 Calibrations and performance checks of the analytical system were conducted regularly using commercial pure methane standards. The coefficient of variation determined for the analytical procedure was less than 2%.

Stable carbon isotope signatures

390 Three sedimentary gas samples each extracted from two gravity cores taken close to flare origins (GC-1: station PS81/280-1 in cross-shelf Trough 6, Fig. 3a; GC-2: station PS81/284-1 in Cumberland Bay, Fig. 3b) were analyzed for stable carbon isotope ratios of methane. The samples were obtained from depths between 6 and 9 meters below sea floor (mbsf), which was below the actual depth of the sulfate-methane transition (Chapter 9 in Bohrmann⁶³), and, thus, should not have been
395 influenced by potential anaerobic oxidation of methane processes. Sediment (3 ml) was sampled from the bottom of each of the freshly cut core sections using cut-off syringes and transferred into 20 ml glass vials prefilled with 5 ml of 1 M NaOH. The gas was sampled for onboard methane concentration analyses and shore-based measurements of its stable isotope signature. Analysis of stable C isotope signatures of CH₄ was conducted in the commercial GEO-data GmbH laboratory
400 (Garbsen, Germany). Stable C isotope signatures are reported in δ -notation in parts permil (‰), relative to the Vienna PeeDee Belemnite (V-PDB) standard for carbon isotopes. The reproducibility of stable carbon isotope determinations is estimated at $\pm 0.1\%$.

References

1. Judd, A. & Hovland, M. *Seabed Fluid Flow*. 475 (Cambridge University Press, 2007).

- 405 2. Suess, E. in *Handbook Of Hydrocarbon And Lipid Microbiology* (Timmis, K. N.) 186–203 (Springer, 2010).
3. Domack, E. *et al.* A chemotrophic ecosystem found beneath Antarctic Ice Shelf. *Eos*, **86**, 269 (2005).
- 410 4. Niemann, H. *et al.* Biogeochemistry of a low-activity cold seep in the Larsen B area, western Weddell Sea, Antarctica. *Biogeosciences* **6**, 2383–2395 (2009).
5. Van Dover, C. L., German, C. R., Speer, K. G., Parson, L. M. & Vrijenhoek, R. C. Evolution and biogeography of deep-sea vent and seep invertebrates. *Science* **295**, 1253–7 (2002).
6. Bohrmann, G., Chin, C. & Petersen, S. Hydrothermal activity at Hook Ridge in the Central Bransfield Basin, Antarctica. *Geo-Mar. Lett.* **18**, 277–284 (1999).
- 415 7. Aquilina, A. *et al.* Geochemical and visual indicators of hydrothermal fluid flow through a sediment-hosted volcanic ridge in the Central Bransfield Basin (Antarctica). *PLoS ONE* **8**, (2013).
8. Rogers, A. D. *et al.* The discovery of new deep-sea hydrothermal vent communities in the southern ocean and implications for biogeography. *PLoS Biology* **10**, e1001234 (2012).
- 420 9. Amon, D. J. *et al.* The discovery of a natural whale fall in the Antarctic deep sea. *Deep-Sea Res. Pt II* **92**, 87–96 (2013).
10. Rogers, A. D. & Linse, K. in *Biogeographic Atlas of the Southern Ocean* (De Broyer C. *et al.*) 2–6 (Scientific Committee on Antarctic Research, 2012).
- 425 11. McGinnis, D. F., Greinert, J., Artemov, Y., Beaubien, S. E. & Wüest, A. Fate of rising methane bubbles in stratified waters: How much methane reaches the atmosphere? *J. Geophys. Res.* **111**, C09007 (2006).
12. Römer, M., Sahling, H., Pape, T., Bohrmann, G. & Spieß, V. Quantification of gas bubble emissions from submarine hydrocarbon seeps at the Makran continental margin (offshore Pakistan). *J. Geophys. Res.* **117**, C10015 (2012).
- 430 13. Mau, S., Heintz, M. B. & Valentine, D. L. Quantification of CH₄ loss and transport in dissolved plumes of the Santa Barbara Channel, California. *Cont. Shelf Res.* **32**, 110–120 (2012).
14. Schneider Von Deimling, J. *et al.* Quantification of seep-related methane gas emissions at Tommeliten, North Sea. *Cont. Shelf Res.* **31**, 867–878 (2011).
- 435 15. Schmale, O., Beaubien, S. E., Rehder, G., Greinert, J. & Lombardi, S. Gas seepage in the Dnepr paleo-delta area (NW-Black Sea) and its regional impact on the water column methane cycle. *J. Marine Syst.* **80**, 90–100 (2010).
16. Westbrook, G. K. *et al.* Escape of methane gas from the seabed along the West Spitsbergen continental margin. *Geophys. Res. Lett.* **36**, L16608 (2009).
- 440 17. Gentz, T. *et al.* A water column study of methane around gas flares located at the West Spitsbergen continental margin. *Cont. Shelf Res.* (2013).

18. Greinert, J., McGinnis, D. F., Naudts, L., Linke, P. & De Batist, M. Atmospheric methane flux from bubbling seeps: Spatially extrapolated quantification from a Black Sea shelf area. *J. Geophys.Res.* **115**, C01002 (2010).
- 445 19. Shakhova, N. *et al.* Extensive methane venting to the atmosphere from sediments of the East Siberian Arctic Shelf. *Science* **327**, 1246–50 (2010).
20. Cunningham, A. P., Barker, P. F. & Tomlinson, J. S. Tectonics and sedimentary environment of the North Scotia Ridge region revealed by side-scan sonar. *J. Geol. Soc.London* **155**, 941–956 (1998).
- 450 21. Dalziel I. W. D., Dott R. H. Jr, Winn R. D. Jr, Bruhn R. L. Tectonic relations of South Georgia Island to the southernmost Andes. *Bull. Geol. Soc. Am.* **86**, 1034–1040 (1975).
22. Forsyth, D. W. Fault plane solutions and tectonics of the South Atlantic and Scotia Sea. *J. Geophys. Res.* **80**, 1429–1443 (1975).
23. Ludwig, W. J. & Rabinowitz, P. D. The collision complex of the North Scotia Ridge. *J. Geophys.Res.* **87**, 3731 (1982).
- 455 24. Pelayo, A. & Wiens, D. Seismotectonics and relative plate motions in the Scotia Sea region. *J. Geophys.Res.* **94**, 7293–7320 (1989).
25. Curtis, M. L., Flowerdew, M. J., Riley, T. R., Whitehouse, M. J. & Daly, J. S. Andean sinistral transpression and kinematic partitioning in South Georgia. *J. Struct.Geol.* **32**, 464–477 (2010).
- 460 26. Graham, A. G. C. *et al.* A new bathymetric compilation highlighting extensive paleo-ice sheet drainage on the continental shelf, South Georgia, sub-Antarctica. *Geochem. Geophys. Geosy.* **9**, Q07011 (2008).
27. Simpson, P. & Griffiths, D. H. in *Antarctic Geoscience* (Craddock, C.) 185 – 191 (Int. Union of Geol. Sci., 1982).
- 465 28. Thorpe, S. E., Heywood, K. J., Brandon, M. A & Stevens, D. P. Variability of the southern Antarctic Circumpolar Current front north of South Georgia. *J. Marine Syst.* **37**, 87–105 (2002).
29. Young, E. F., Meredith, M. P., Murphy, E. J. & Carvalho, G. R. High-resolution modelling of the shelf and open ocean adjacent to South Georgia, Southern Ocean. *Deep-Sea Res.Pt II* **58**, 1540–1552 (2011).
- 470 30. Meredith, M. P. *et al.* Variability in hydrographic conditions to the east and northwest of South Georgia, 1996–2001. *J. Marine Syst.* **53**, 143–167 (2005).
31. Whitehouse, M. J. *et al.* Rapid warming of the ocean around South Georgia, Southern Ocean, during the 20th century: Forcings, characteristics and implications for lower trophic levels. *Deep-Sea Res. Pt I* **55**, 1218–1228 (2008).
- 475 32. Borrione, I. & Schlitzer, R. Distribution and recurrence of phytoplankton blooms around South Georgia, Southern Ocean. *Biogeosciences* **10**, 217–231 (2013).

33. Jones, E. M., Bakker, D. C. E., Venables, H. J. & Watson, A. J. Dynamic seasonal cycling of inorganic carbon downstream of South Georgia, Southern Ocean. *Deep-Sea Res. Pt II* **59-60**, 25–35 (2012).
- 480 34. Campbell, K. A. Hydrocarbon seep and hydrothermal vent paleoenvironments and paleontology: Past developments and future research directions. *Palaeogeogr. Palaeocl.* **232**, 362–407 (2006).
35. Bachraty, C., Legendre, P. & Desbruyères, D. Biogeographic relationships among deep-sea hydrothermal vent faunas at global scale. *Deep-Sea Res. Pt I* **56**, 1371–1378 (2009).
- 485 36. James E., McKenna Jr. Trophic relationships within the Antarctic demersal fish community of South Georgia Island. *Fish. B.-NOAA* **89**, 643–654 (1991).
37. Hogg, O. T., Barnes, D. K. A. & Griffiths, H. J. Highly diverse, poorly studied and uniquely threatened by climate change: An assessment of marine biodiversity on South Georgia’s continental shelf. *PLoS ONE* **6**, (2011).
- 490 38. Jones, C. D. *et al.* Diversity, relative abundance, new locality records and population structure of Antarctic demersal fishes from the northern Scotia Arc islands and Bouvetøya. *Polar Biol.* **31**, 1481–1497 (2008).
39. Sahling, H. *et al.* Depth-related structure and ecological significance of cold-seep communities—a case study from the Sea of Okhotsk. *Deep-Sea Res. Pt I* **50**, 1391–1409 (2003).
- 495 40. Little, C., Campbell, K. & Herrington, R. Why did ancient chemosynthetic seep and vent assemblages occur in shallower water than they do today? Comment. *Int. J. Earth Sci.* **91**, 149–153 (2002).
41. Orange, D. L., Yun, J., Maher, N., Barry, J. & Greene, G. Tracking California seafloor seeps with bathymetry, backscatter and ROVs. *Cont. Shelf Res.* **22**, 2273–2290 (2002).
- 500 42. Grant, A., Levy, E., Lee, K. & Moffat, J. Pisces IV research submersible finds oil on Baffin Shelf. *Current Research, Part A, Geological Survey of Canada* **86**, 65–59 (1986).
43. Levy, E. & Ehrhardt, M. Natural seepage of petroleum at Buchan Gulf, Baffin Island. *Mar. Chem.* **10**, 355–364 (1981).
- 505 44. Forwick, M., Baeten, N. J. & Vorren, T. O. Pockmarks in Spitsbergen fjords. *Norw. J. Geol.* **89**, 65–77 (2009).
45. Hodgson, D. A. *et al.* Glacial history of sub-Antarctic South Georgia based on the submarine geomorphology of its fjords. *Quaternary Sci. Rev.*
46. Platt, H. M. Sedimentation and the distribution of organic matter in a sub-Antarctic marine bay. *Estuar. Coast. Mar. Sci.* **9**, 51–63 (1979).
- 510 47. Claypool, G. & Kvenvolden, K. Methane and other hydrocarbon gases in marine sediment. *Annu. Rev. Earth Pl. Sc.* **11**, 299–327 (1983).

48. Meredith, M. P. An anticyclonic circulation above the Northwest Georgia Rise, Southern Ocean. *Geophys. Res. Lett.* **30**, 2061 (2003).
- 515 49. Atkinson, a *et al.* South Georgia, Antarctica: a productive, cold water, pelagic ecosystem. *Mar. Ecol.-Prog. Ser.* **216**, 279–308 (2001).
50. Schlitzer, R. Carbon export fluxes in the Southern Ocean: results from inverse modeling and comparison with satellite-based estimates. *Deep-Sea Res. Pt II* **49**, 1623–1644 (2002).
51. Heeschen, K. U. *et al.* Methane sources, distributions, and fluxes from cold vent sites at Hydrate Ridge, Cascadia Margin. *Global Biogeochem. Cy.* **19**, GB2016 (2005).
- 520 52. Torres, M. E. *et al.* Fluid and chemical fluxes in and out of sediments hosting methane hydrate deposits on Hydrate Ridge, OR, USA: Hydrological provinces. *Earth Planet. Sc. Lett.* **201**, 525–540 (2002).
- 525 53. Hornafius, J. The world's most spectacular marine hydrocarbon seeps (Coal Oil Point, Santa Barbara Channel, California): Quantification of emissions. *J. Geophys. Res.* **104**, 20,703 – 20,711 (1999).
54. Nikolovska, A., Sahling, H. & Bohrmann, G. Hydroacoustic methodology for detection, localization, and quantification of gas bubbles rising from the seafloor at gas seeps from the eastern Black Sea. *Geochem. Geophys. Geosy.* **9**, Q10010 (2008).
- 530 55. Pape, T. *et al.* Molecular and isotopic partitioning of low-molecular-weight hydrocarbons during migration and gas hydrate precipitation in deposits of a high-flux seepage site. *Chem. Geol.* **269**, 350–363 (2010).
56. Römer, M. *et al.* Geological control and magnitude of methane ebullition from a high-flux seep area in the Black Sea—the Kerch seep area. *Mar. Geol.* **319-322**, 57–74 (2012).
- 535 57. Leifer, I. & Patro, R. K. The bubble mechanism for methane transport from the shallow sea bed to the surface: A review and sensitivity study. *Cont. Shelf Res.* **22**, 2409–2428 (2002).
58. Wüest, A., Brooks, N. H. & Imboden, D. M. Bubble plume modeling for lake restoration. *Water Resour. Res.* **28**, 3235–3250 (1992).
59. Leifer, I. & Judd, a. G. Oceanic methane layers: the hydrocarbon seep bubble deposition hypothesis. *Terra Nova* **14**, 417–424 (2002).
- 540 60. Greinert, J. & McGinnis, D. F. Single bubble dissolution model – The graphical user interface SiBu-GUI. *Environ. Modell. Softw.* **24**, 1012–1013 (2009).
61. Greinert, J., Artemov, Y., Egorov, V., Debatist, M. & McGinnis, D. 1300-m-high rising bubbles from mud volcanoes at 2080m in the Black Sea: Hydroacoustic characteristics and temporal variability. *Earth Planet. Sc. Lett.* **244**, 1–15 (2006).
- 545 62. Valentine, D., Blanton, D., Reeburgh, W. S. & Kastner, M. Water column methane oxidation adjacent to an area of active hydrate dissociation, Eel River Basin. *Geochim. Cosmochim. Ac.* **65**, 2633–2640 (2001).

63. Bohrmann, G. The expedition of the research vessel “Polarstern” to the Antarctic in 2013 (ANT-XXIX/4). *Berichte zur Polar- und Meeresforschung* **668**, 145 p. (2013).
- 550 64. Caress, D. W. *et al.* Repeat bathymetric surveys at 1-metre resolution of lava flows erupted at Axial Seamount in April 2011. *Nat. Geosci.* **5**, 1–6 (2012).
65. Fretwell, P. T., Tate, A. J., Deen, T. J. & Belchier, M. Compilation of a new bathymetric dataset of South Georgia. *Antarct. Sci.* **21**, 171 (2008).
- 555 66. Rehder, G., Keir, R. S., Suess, E. & Rhein, M. Methane in the northern Atlantic controlled by microbial oxidation and atmospheric history. *Geophys. Res. Lett.* **26**, 587–590 (1999).
67. MacDonald, D. I. M. & Storey, B. C. *South Georgia, BAS GEOMAP Series, Sheet 1, scale 1:250,000*. 63 (British Antarctic Survey, 1987).

Acknowledgements

560 We greatly appreciate the shipboard support from the master and crew of the research vessel Polarstern during cruise ANT-XXIX/4. This work was supported by the Deutsche Forschungsgemeinschaft (DFG) in the framework of the priority program ‘Antarctic Research with comparative investigations in Arctic ice areas’ by a grant to BO 1049/19 and through the DFG-Research Center / Cluster of Excellence „The Ocean in the Earth System“. AGCG was supported by 565 Natural Environment Research Council (NERC) New Investigator Grant, NEK0005271, and by a fieldwork grant from the UK Quaternary Research Association (QRA) Research Fund. KL was supported by the ChEsSo programme (Consortium Grant NE/DO1249X/1) funded by NERC. CTSL acknowledges travel funds from the Earth Surface Sciences Institute, University of Leeds.

Author contributions

570 M.R. led the authorship of the paper. G.B. was principle scientist of R/V Polarstern ANT-XXIX/4. P.W. and A.G.C.G. took care of the processing of MBES data. G.K. and M.R. operated and analyzed the SBES data. S.M., P.G., and J.R. conducted hydrocasts and water column analyses. C.T.S.L., K.L., Y.M. and M.R. operated the OFOS and analyzed the video material. T.P., P.G. and J.R. provided the gas analyses. All authors contributed to the development of the paper.

575 Figure captions

Fig. 1 a) Plate tectonic overview with the South Georgia microplate (SG) located at the eastern part of the North Scotia Ridge. SAM: South American Plate, SCO: Scotia Plate, SAN: Sandwich Plate, ANT:

Antarctic Plate (modified after Cunningham et al.²⁰). b) Map of the main tectonic structures of the South Georgia crustal block (after MacDonald et al.⁶⁷). The shelf morphology is characterized by at least ten cross-shelf troughs sourcing at the fjords of the island (yellow areas; Graham et al.²⁶).

Fig. 2 a) Echogram recorded with the single beam echosounder (SBES) illustrating a flare composed of numerous oblique high-backscatter traces representing uprising gas bubbles. The footprint of the SBES at a water depth of ~380 mbsl corresponds to ~30 m to the width of the flare signal at the sea floor (white line). b) SBES echogram combining the water column data and the subbottom information (using 18 and 3.5 kHz frequencies, respectively). Gas emission sites are characterized by acoustic blanking in the subsurface (gas chimneys) and emissions of free gas in the water column causing hydroacoustic flares. For locations see Figs. 3a and b.

Fig. 3 a) Map showing the shelf bathymetry with its characteristic cross-shelf troughs in combination with the ship track (black line) and flare positions (red dots) detected during R/V Polarstern cruise ANT-XXIX/4. Cross-shelf Troughs 1-7 at the northern shelf have been crossed in order to detect free gas in the subbottom and water column. Additionally, two fjords were investigated: the Possession Bay, where Trough 4 is sourced, and the Cumberland Bay, which is directly connected to Trough 5. b) Detailed map of the Cumberland Bay with the processed bathymetric data acquired during cruise ANT-XXIX/4. More than 75 flares were detected during the surveys within the fjord system.

Fig. 4 Three profiles recorded with SBES combining subbottom (3.5 kHz) and water column (18 kHz) information. Flares are repainted in red. For locations see Figs. 3a and b. a) Profile 1 shows an echogram crossing the cross-shelf Trough 4. Several flares were detected, but the majority showed a discontinuous pattern most probably caused by pulsing gas bubble emissions. b) Profile 2 shows an echogram at cross-shelf Trough 6. In contrast to the shallow banks lacking visible sediment strata in the subbottom, the troughs are characterized by sediment accumulation. c) Profile 3 shows an echogram recorded during entering of the Cumberland Bay and crossing the 'Cumberland Bay flare'.

Several acoustic chimneys characterized by vertical blanking zones illustrate up-rising free gas in the subbottom (red outlines with arrows) and additionally, three flares prove the emission of gas bubbles into the water column.

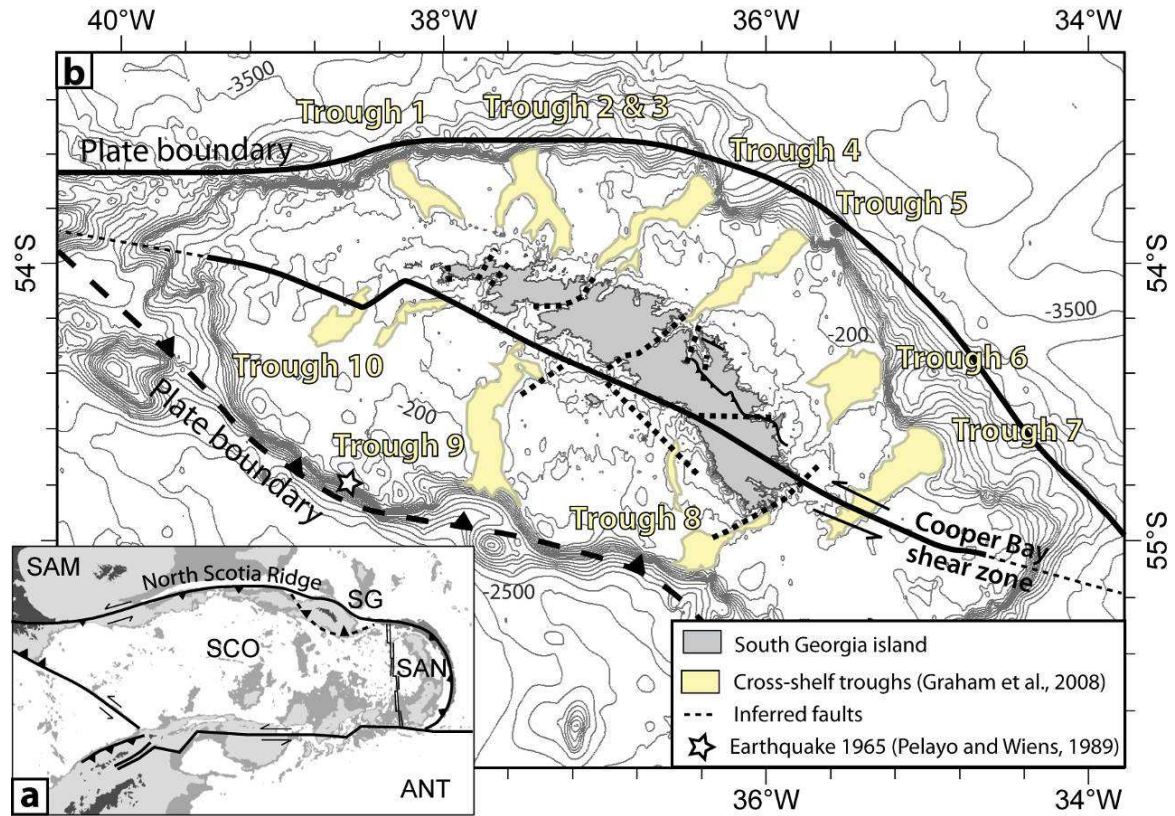
Fig. 5 a) Bathymetric map from ship-based swath echosounder recordings with the dive track of the Ocean Floor Observation System (OFOS; station PS81/285-1) passing two areas, where hydroacoustic investigations indicated gas bubble emissions from the sea floor (light red circles). Rising gas bubbles were recognized in both areas and whitish patches on the sea floor additionally proved the position of the seep sites (white dots).

Fig. 6 a) Sea floor picture taken at the Cumberland Bay Flare with the high-resolution video camera mounted on the frame of the Ocean Floor Observation System (OFOS) and showing an elongated mounded structure at the sea floor characterized by whitish color, probably representing microbial mats. b) Sea floor image taken at the northwestern flare area demonstrates the occurrence and intercalation of white colored and additionally dark grey colored patches. For locations see Figs. 3b and 5.

Fig. 8 Water column profile illustrating selected data recorded during three CTD casts acquired. Stations CTD-1 (colored dashed lines) and CTD-2 (colored solid lines) were located within the Cumberland Bay and CTD-3 (black lines) seaward the fjord mouth (see Fig. 3b). Elevated methane concentrations were measured in particular in the lowermost ~100 m at the two Cumberland Bay stations taken close to hydroacoustically detected flares. Bottom waters at that depth were characterized by low temperatures, beam transmissions and dissolved oxygen concentrations.

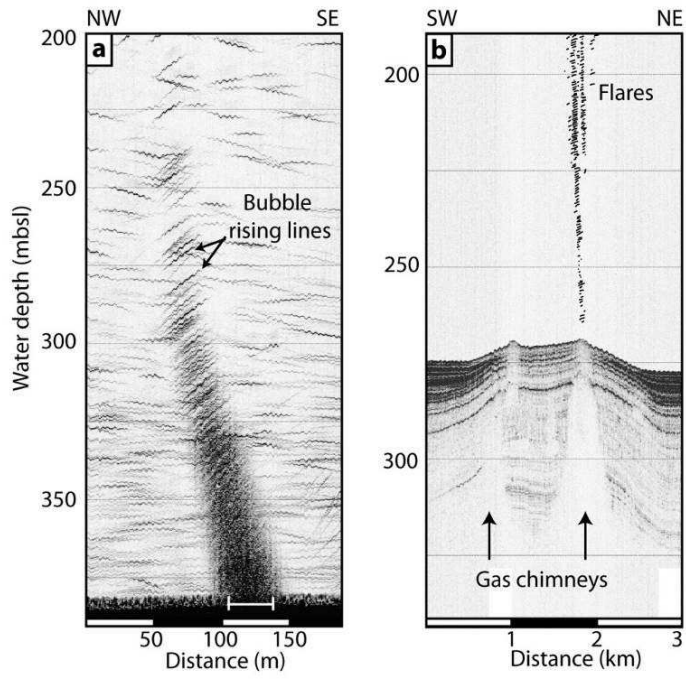
Supplementary Fig. S3 Temperature-Salinity diagram of the data from the three CTD stations during ANT-XXIX/4. T-S condition in surface waters at stations CTD-1 and CTD-2 located in the Cumberland Bay clearly differed from those at station CTD-3 positioned seaward (for locations see Fig. 3b).

Fig. 1



630

Fig. 2



635 Fig. 3

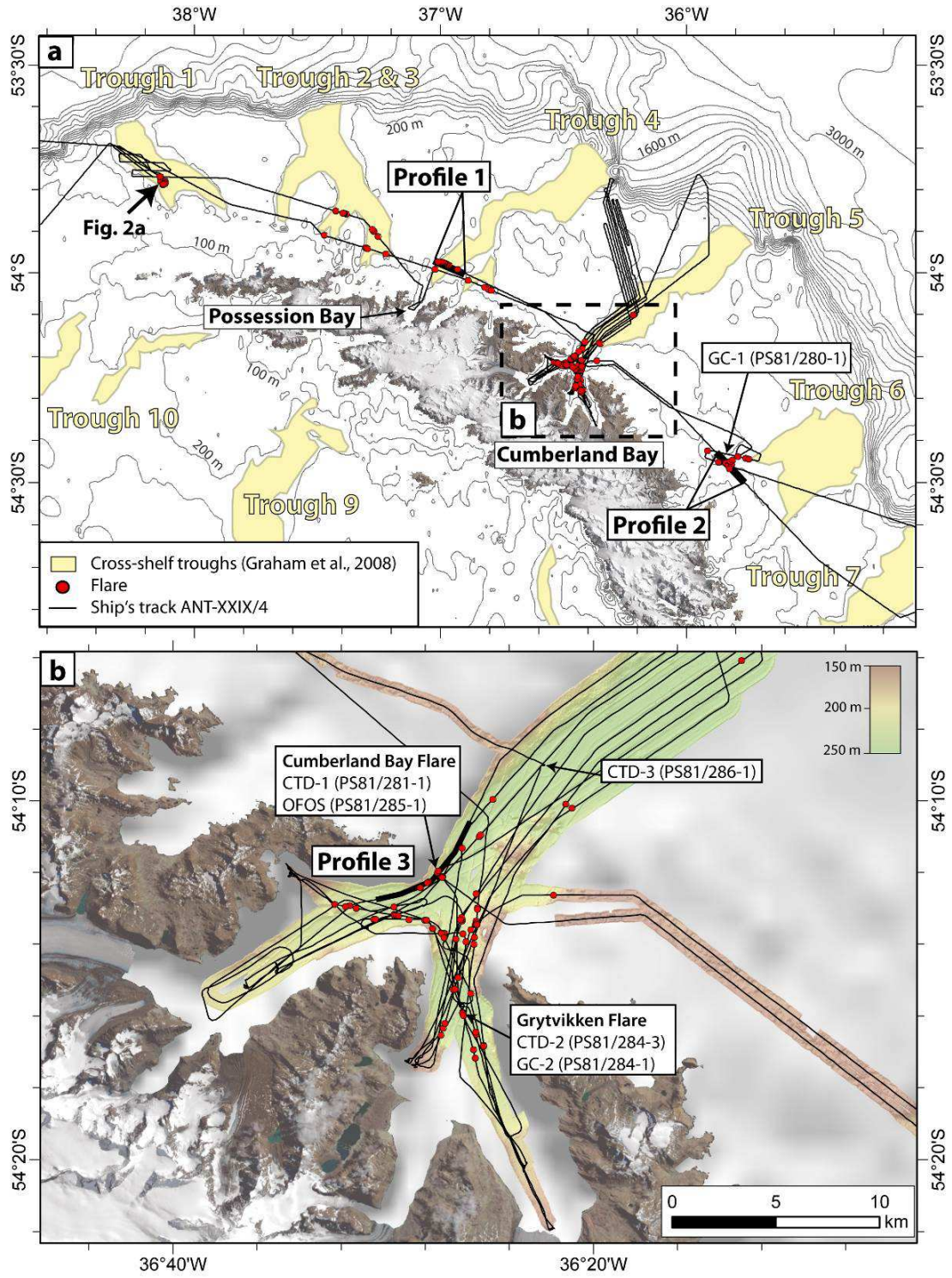


Fig. 4

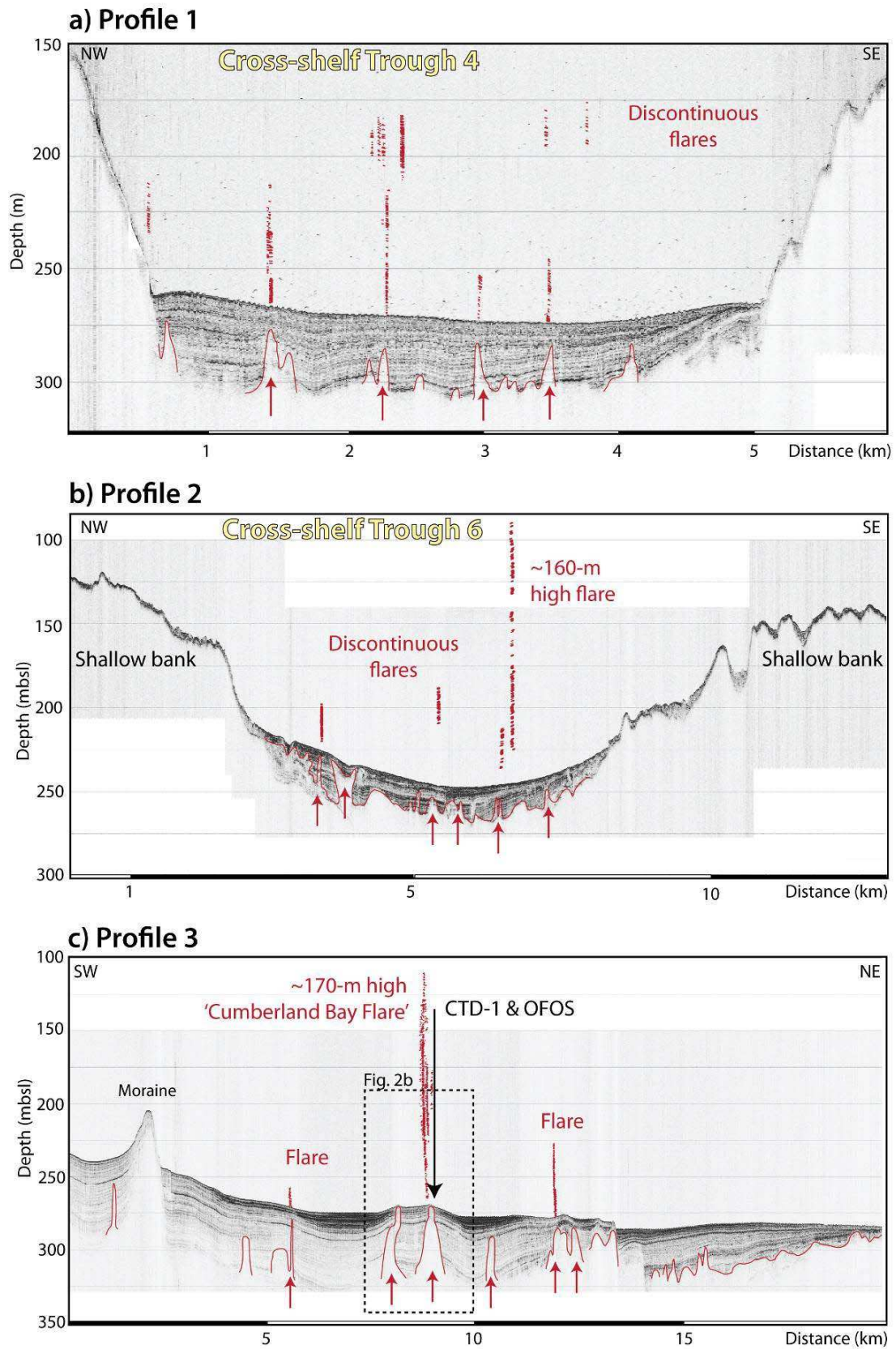


Fig. 5

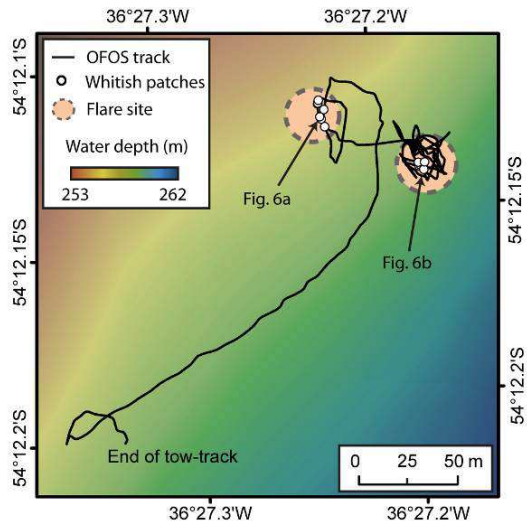


Fig. 6

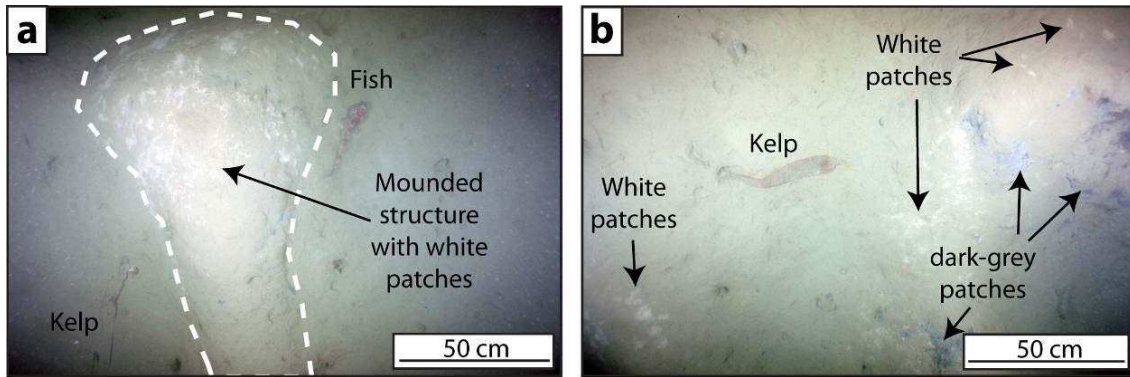
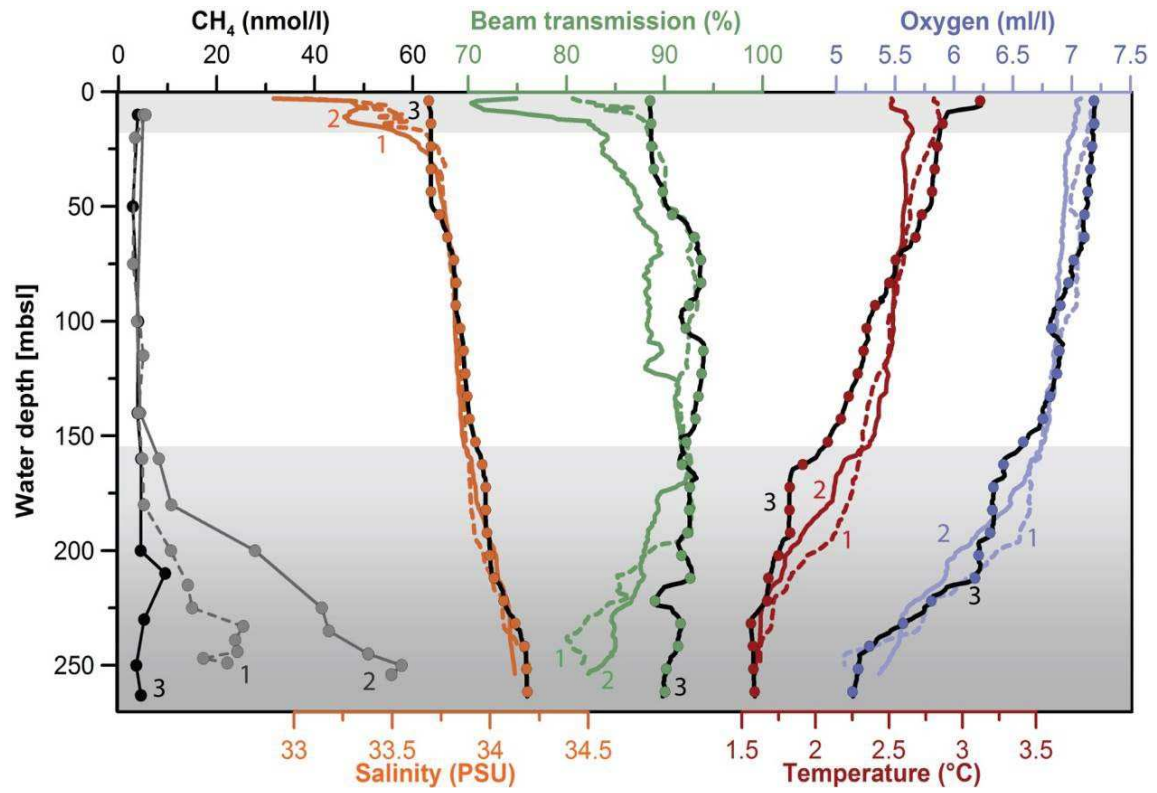


Fig. 7



650